ACS APPLIED MATERIALS & INTERFACES

Research Article

Cite This: ACS Appl. Mater. Interfaces 2019, 11, 36580−36588

www.acsami.org

Enhancement in Desalination Performance of Battery Electrodes via Improved Mass Transport Using a Multichannel Flow System

Jiho Lee,[†,⊥] Jaehan Lee,[‡,⊥] Jaewuk Ahn,[†] Kyusik Jo,[†] Sung Pil Hong,[†] Choonsoo Kim,[§] Changha Lee,[†] and Jeyong Yoon*[,†,∥]

[†]School of Chemical and Biological Engineering, College of Engineering, Institute of Chemical Process, Seoul National University (SNU), 1 Gwanak-ro, Gwanak-gu, Seoul 08826, Republic of Korea

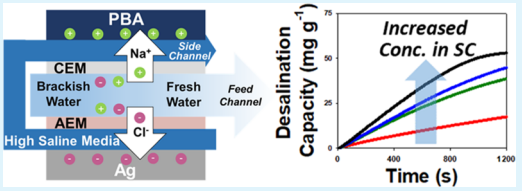
[‡]Department of Biological and Chemical Engineering, College of Science and Technology, Hongik University, 2639 Sejong-ro, Sejong-si 30016, Republic of Korea

[§]Department of Environmental Engineering and Institute of Energy/Environment Convergence Technologies, Kongju National University, 1223-23, Cheonan-daero, Cheonan-si 31080, Republic of Korea

[∥]Korea Environment Institute, 370 Sicheong-daero, Sejong-si 30147, Republic of Korea

Supporting Information

ABSTRACT: Desalination technologies have heavily been investigated to utilize the abundant salt water on Earth due to the global freshwater shortage. During recent years, the desalination battery (DB) has attracted attention for its low-cost, eco-friendly, and energy-efficient characteristics. However, the current DB system is subject to inevitable performance degradation because of the mass-transfer limitation at the electrode−electrolyte interface, particularly when the system is used to treat brackish water. Here, we present a novel strategy to overcome the intrinsic mass-transfer limitation of DB in brackish water using an effective cell design based on a multichannel flow system. Compared to the conventional DB that consists of one feed channel, the multichannel desalination battery (MC-DB) is configured using two side channels introducing a highly concentrated solution to the electrodes and one middle feed channel for water desalination. The MC-DB showed a desalination capacity of 52.9 mg g^{-1} and a maximum salt removal rate of 0.0576 mg g^{-1} s^{-1} (production rate of 42.3 g m^{-2} h^{-1}) when a salinity gradient between the feed streams in the middle (10 mM NaCl) and side (1000 mM NaCl) channels was present, which were 3-fold higher than those in the case with no salinity gradient. In addition, the high concentration solution in the side channel significantly enhanced the rate capability of MC-DB, allowing the system to operate under a high current density of 40 A m^{-2} with a desalination capacity of 34.1 mg g^{-1}. Considering the effect of electrolyte concentration on the battery electrode performance through electrochemical characterization, the highly saline medium at the side channel in the MC-DB creates an optimal environment for the battery electrode to fully capitalize the high desalination capacity, salt removal rate, and capacity retention of the battery electrodes.



KEYWORDS: *water treatment, multichannel flow system, electrochemical ion separation, desalination battery, Prussian blue analogue*

Downloaded via HONGIK UNIV on October 10, 2019 at 05:08:08 (UTC).
See https://pubs.acs.org/sharingguidelines for options on how to legitimately share published articles.

1. INTRODUCTION

Water scarcity has become a severe global issue because of rapid world population growth and industrialization. To secure a clean water supply, desalination has been investigated as approximately 97% of water resources on Earth contain high salt concentrations. During recent years, electrochemical ion separation technologies such as electrodialysis, capacitive deionization (CDI), and desalination battery (DB) have been intensively studied for their advantages of a high water recovery rate, environmentally benign materials, and energy-efficient characteristics.[1−8] Among them, DB is a highly attractive technology because of its high desalination capacity and energy efficiency.[9−13] Typically, a DB consists of a pair of cation- and anion-capturing electrodes that undergo a reversible electrochemical reaction to remove/release ions as a potential difference is applied. Inspired by aqueous Na-ion battery materials, the DB has extensively progressed through employing materials such as cobalt oxide,[14] sodium manganese oxide,[15,16] sodium titanium phosphates,[13,17] and Prussian blue and its analogues,[10−12] which have a large specific capacity via storing ions in the electrode bulk crystal structure. Using these materials, high desalination performance greater than 30 NaCl mg g^{-1} of electrodes has been achieved, which is significantly higher than that of carbon-based CDI (∼25 NaCl mg g^{-1} of electrodes).[18−26] In addition, the small cell voltage window and low self-discharging properties compared to those of the carbon materials allow the DB to be highly energy efficient.[16]

However, the conventional DB system suffers from inevitable performance degradation due to the mass-transfer limitation, particularly, when used to treat brackish water.

Received: June 13, 2019
Accepted: September 18, 2019
Published: September 27, 2019

© 2019 American Chemical Society

DOI: 10.1021/acsami.9b10003
ACS Appl. Mater. Interfaces 2019, 11, 36580−36588

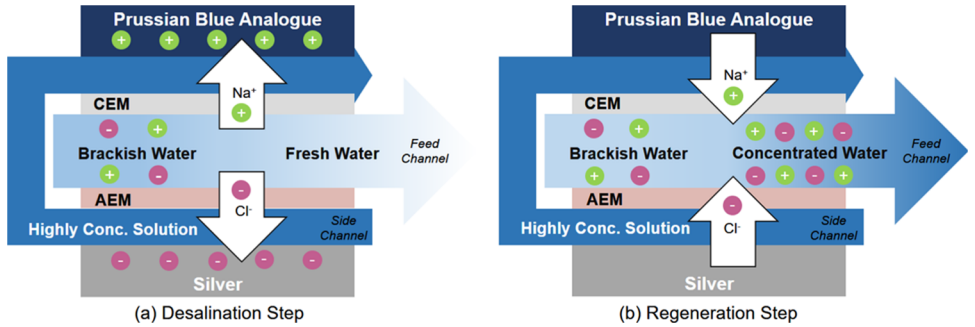


Figure 1. Conceptual diagram of a multichannel desalination battery (MC-DB) divided into (a) desalination step (discharging) and (b) regeneration step (charging). The side and the middle feed channels were divided by the cation and anion exchange membranes. In the side channels, a highly concentrated solution was supplied.

Unlike a highly concentrated electrolyte (>1 M) in battery system for energy storage, the brackish water (500−2000 ppm total dissolved solids)[27] provides limited amount of accessible ions at the electrode−electrolyte interface in the DB system. Hence, the DB system is kinetically slow and has to operate under a low current density (<10 A m^{-2}) to fully utilize the ion-storage capacity of the battery during desalination processes.[10,28,29] Although various attempts have been made to improve the rate capability of the battery materials through particle size control,[30,31] mesoporous structure formation,[32,33] and combining with carbon nanomaterials,[34−36] an innovative solution is required for the intrinsic mass-transfer limitation that lowers the DB electrode performance.

Here, we propose a novel strategy to overcome the mass-transfer limitation in the DB using a multichannel flow system design (denoted as a multichannel desalination battery (MC-DB)) that can independently control the solution surrounding the electrodes and the target brackish water. As shown in Figure 1, the MC-DB consists of two side and one middle flow channels separated by cation and anion exchange membranes, a cell configuration benchmarked to the multichannel flow membrane CDI system reported in our previous work.[37−39] In this system, highly concentrated salt water (1000 mM NaCl) was supplied to the Prussian blue analogue (PBA) and silver (Ag) electrodes in the side channels. Low-saline media (10 mM NaCl) was prepared to depict a brackish water condition and fed to the middle channel for desalination. As a potential difference is applied between the two battery electrodes, sodium (Na^+) and chloride (Cl^-) ions in the side channels were captured via redox reactions, whereas ions present in the middle channel selectively migrated through the ion-exchange membranes. The captured ions were released into the middle channel by applying a reverse cell voltage. In this study, the influence of the NaCl concentration supplied to the side channels on the desalination performance was evaluated under various operating conditions. In particular, a CDI Ragone plot was constructed to further investigate the rate capability of the MC-DB system. In addition, changes in the electrochemical properties of the battery materials with respect to electrolyte concentration were investigated to explain the high desalination performance of the MC-DB system.

2. EXPERIMENTAL METHODS

2.1. Material Synthesis. Nickel hexacyanoferrate (NiHCF), a well-known type of Prussian blue analogue, was prepared via a controlled crystallization reaction with nickel chloride ($NiCl_2$), sodium citrate (Na-citrate), and sodium ferrocyanide ($Na_4Fe(CN)_6$) to obtain an ordered cubic particle.[11] One hundred milliliters of 0.05 M $NiCl_2$ and 0.35 M Na-citrate were mixed with 100 mL of 0.05 M $Na_4Fe(CN)_6$ solution under rapid stirring. Under ambient conditions, the crystallization was conducted for 48 h and then aged overnight. The resulting precipitants were filtered and thoroughly washed with demineralized water and ethanol. The synthesized particles were dried in a vacuum oven at 60 °C to eliminate the remaining solvent. The Ag particles were purchased from Henqiu Technology Co., Ltd., China. The prepared particles were characterized using field emission scanning electron microscopy (JEOL JSM 6700 F), high-resolution resolution transmission electron microscopy (HRTEM; JEM-3010), and X-ray powder diffraction (XRD; D8 Discover). All reagents were purchased from Sigma-Aldrich Corporation and used without further treatment.

2.2. Electrode Fabrication. The NiHCF and Ag electrodes were fabricated by mixing active material (NiHCF and Ag particles), carbon black (Super P, Timcal, Switzerland), and poly-(tetrafluoroethylene) (Sigma-Aldrich) in an 8:1:1 weight ratio with the addition of an ethanol solvent on a mortar. The resulting slurry was pressed using a roll press machine to obtain sheet-type electrodes. The fabricated electrodes were dried using a vacuum oven at 60 °C overnight to remove the remaining solvent. Rectangular NiHCF (area: 2.5 × 2.5 cm^2, thickness: ∼300 μm, weight: 177 ± 7 mg) and Ag (area: 2.5 × 2.5 cm^2, thickness: ∼150 μm, weight: 194 ± 2 mg) were used as positive and negative electrodes, respectively. NiHCF was attached to a graphite sheet (thickness: 0.20 mm; Sigma-Aldrich) using carbon paint (DAG-T-502; Ted Pella) and preoxidized at 1.0 V (vs Ag/AgCl KCl sat.) to deintercalate the sodium ions in 1000 mM NaCl before the desalination test.

2.3. Electrochemical Characterization of the Prepared Electrodes. The electrochemical properties of the NiHCF and Ag electrodes were examined by cyclic voltammetry (CV) and galvanostatic charging/discharging tests with a potentiostat (VersaSTAT 3, Princeton Applied Research) and a battery cycler (WBCS3000, WonA Tech Co.), respectively. The CV and galvanostatic charging/discharging tests were conducted using a three-electrode system at various NaCl electrolyte concentrations of 10, 100, 500, and 1000 mM. The NiHCF and Ag electrodes were used as the working electrodes (diameter = 9 mm), an Ag electrode was employed as the counter electrode (diameter = 18 mm), and a KCl-saturated Ag/AgCl electrode was used as a reference electrode. A glass microfiber filter was used as a separator (thickness: ∼110 μm; Whatman).

In addition, a cyclability test of the NiHCF/Ag configuration was conducted in a two-electrode system. The NiHCF and Ag electrodes were used as positive and negative electrodes (d = 9 mm), respectively. Various current densities ranging from 5 to 30 A m^{-2} were tested to investigate the rate performance of NiHCF/Ag. The cycling ability of the NiHCF/Ag cell was conducted for 100 cycles at a current density of 30 A m^{-2} based on the geometrical area of the cell in a voltage window of 0.0−0.8 V in 10 and 1000 mM NaCl solutions.

2.4. Multichannel Desalination Battery System Assembly. The MC-DB system was configured as shown in Figure 1. The system consisted of two side channels (2.5 × 2.5 × 1.0 cm^3) and one feed

DOI: 10.1021/acsami.9b10003
ACS Appl. Mater. Interfaces 2019, 11, 36580−36588

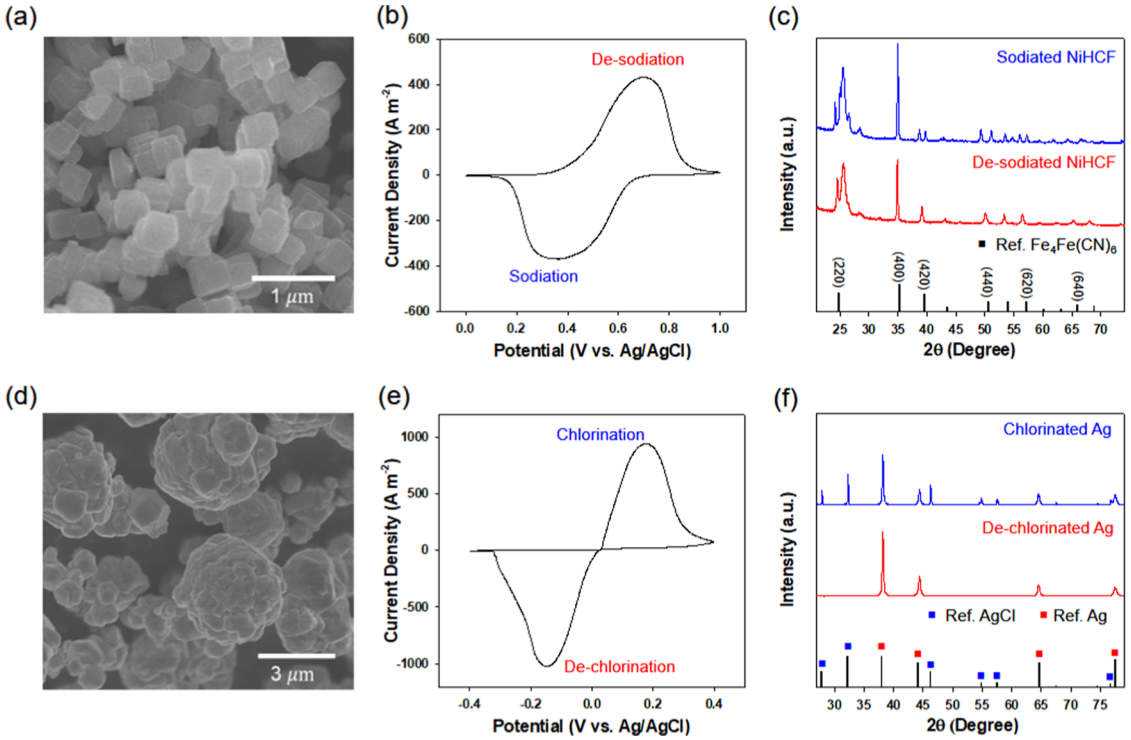


Figure 2. Scanning electron microscopy (SEM) image of (a) nickel hexacyanoferrate (NiHCF) and (d) silver (Ag) particles. Cyclic voltammogram of (b) NiHCF and (e) Ag electrodes in 1000 mM NaCl electrolyte (scan rate: 2 mV s^{-1}). X-ray diffraction (XRD) peaks of (c) sodiated and desodiated NiHCF with $Fe_4Fe(CN)_6$ reference (JCPDS 52-1907) and (f) chlorinated and dechlorinated Ag with their references of Ag (JCPDS 01-1164) and AgCl (JCPDS 31-1238).

channel (2.5 × 2.5 × 0.3 cm^3) formulated by stacking cation- and anion-exchange membranes (Selemion, Japan) and mesh spacers. The active area of the cell was 6.25 cm^2, and a graphite current collector was used. Finally, the two Teflon endplates were used to cover the assembled MC-DB system. Electrochemical impedance spectroscopy measurement was conducted to evaluate the internal resistance of the cell (Figure S8, Supporting Information).

2.5. Desalination Performance Test. To investigate the desalination performance of the MC-DB system, the effect of various operating parameters including the concentration of source water fed to the side channels, applied voltage, and current were tested. Ten millimolar NaCl solution was used to replicate brackish water and fed to the middle feed (F) channel; NaCl solutions ranging from 10 to 1000 mM were prepared and supplied to the side (S) channel. Note that beyond 1000 mM NaCl, the osmotic pressure between the channels becomes too high and the back-diffusion of ions increases across the ion-exchange membranes. Both the middle and side channel waters were fed at a flow rate of 5 mL min^{-1}. The respective conditions were denoted as $F_{10}S_x$, where x ranged from 10 to 1000 mM. The constant voltage operation was evaluated by applying constant voltages of −1.2/+ 1.2 V, −1.0/+ 1.0 V, and −0.8/+ 0.8 V for the desalination and regeneration steps, respectively. Each step was performed for 20 min. Note that the NiHCF (positive) electrode was negatively biased for the desalination step. The effect of constant current operation was investigated by performing the desalination step under current densities ranging from 5 to 40 A m^{-2} based on the geometrical area of the MC-DB cell until the cutoff voltage of −1.0 V.

The effluent conductivity of the feed channel was monitored using a flow-type conductivity meter (3573-10C, Horiba, Japan). The change in NaCl concentration was obtained by converting the conductivity data. As the indicator for the amount of NaCl was removed, the desalination capacity was calculated by integrating the salt concentration over time during the desalination step, multiplying by the flow rate and molecular weight of NaCl in the feed solution and dividing by the total weight of the two electrodes in eq 1 as follows

$$\text{desalination capacity (mg g}^{-1}) = \frac{M_w \times \int (C_i - C_e) \times \Phi \times dt}{M_e} \quad (1)$$

where M_w is the molecular weight of NaCl (58.44 g mol^{-1}); C_i and C_e are the influent and effluent concentrations (mM), respectively; t is the duration of the desalination step; Φ is the flow rate (mL min^{-1}); and M_e is the total weight of both electrodes (g).

The average salt removal rate was obtained by dividing the accumulated desalination capacity by the duration of the desalination step.

Energy consumption was calculated by dividing the applied electrical energy by the total amount of removed ions during the desalination step. The energy consumption (E) was determined using eq 2 as follows

$$\text{energy consumption per mole of salt removed (kJ mol}^{-1}) = \frac{\int V \times I \times dt}{\int (C_i - C_e) \times \Phi \times dt} \quad (2)$$

where V is the applied voltage and I is the respective current during the desalination step.

The charge efficiency was calculated using eq 3 as follows

$$\text{charge efficiency} = \frac{\int (C_i - C_e) \times \Phi \times dt}{\int I \times dt / F} \quad (3)$$

where F is the Faraday constant (96 485 C mol^{-1}).

Note that as a highly concentrated solution is fed to the side channels, there exists a concentration gradient that induces the back diffusion of salt ions to the feed channel. Under the $F_{10}S_{1000}$ condition, the conductivity of the influent water changed by 7.2 μS cm^{-1}, which corresponds to the ion flux of 14.8 μg min^{-1}. Hence, our system has a small back diffusion that acts against the ion removal flux. To accurately evaluate the desalination efficiency, the

DOI: 10.1021/acsami.9b10003
ACS Appl. Mater. Interfaces 2019, 11, 36580−36588

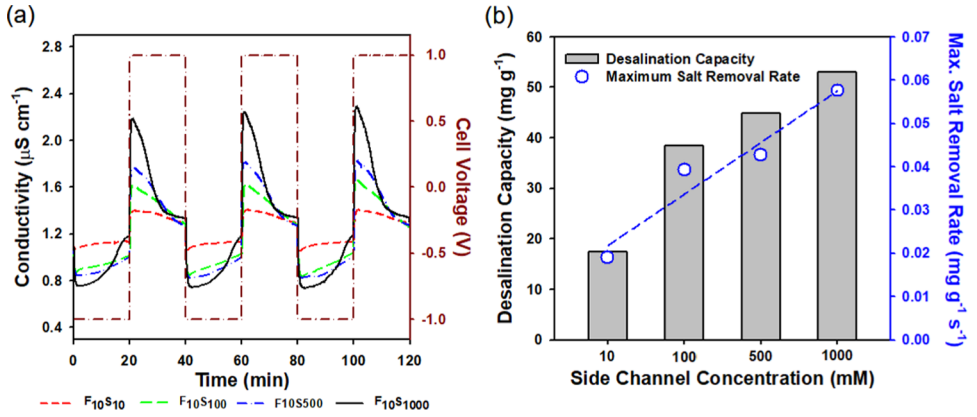


Figure 3. (a) Representative effluent profiles and (b) desalination capacity and maximum salt removal rate of the MC-DB at a feed concentration of 10 mM NaCl in the middle channel (F) with various feed concentrations for the side channel (S) ranging from 10 to 1000 mM ($F_{10}S_x$, x = 10−1000 mM). The side and feed streams were supplied at a flow rate of 5 mL min^{-1}. A desalination test was performed at a constant cell voltage of −1.0 and 1.0 V for the desalination and regeneration steps, respectively.

conductivity baseline was adjusted with the ion flux resulting from back diffusion. In this study, representative results from duplicate or triplicate experiments are presented.

3. RESULTS AND DISCUSSION

3.1. Electrode Characterization. Figure 2 shows the morphologies, electrochemical properties, and X-ray diffraction (XRD) peaks of the NiHCF and Ag electrodes, which are well-known candidates for cation-capturing (e.g., Na^+) and anion-capturing (e.g., Cl^-) electrodes. As shown in Figure 2a, the synthesized NiHCF showed a well-ordered nanocrystal cubic shape with a size distribution of 300−500 nm. The ordered structure of NiHCF is attributed to the kinetically controlled crystallization method as reported by previous studies.[11,40] The Na-citrate acted as a chelating agent to prevent rapid reaction between the metal and hexacyanoferrate ions; hence, controlled nucleation and crystalline growth occurred. In particular, energy-dispersive X-ray spectroscopy intensity peaks from the high-resolution transmission electron microscope (HRTEM) indicate that synthesized NiHCF had a homogeneous distribution of Na, Ni, Fe, C, and N atoms in the crystal structure, implying that NiHCF was well synthesized (Figure S1, Supporting Information).

As seen in the CV curve shown in Figure 2b, the NiHCF electrode exhibited distinct intercalation (sodiation) and deintercalation (desodiation) of sodium ion peaks within the potential range of 0.2−0.6 and 0.5−0.8 V, respectively. The results show the typical shape of the CV curve of the NiHCF electrode resulting from large ionic channels within the host lattice structures that are sufficient to intercalate cations without the desolvation of the hydrated shell.[41,42] Furthermore, this lattice structure can provide a reversible structural distortion from a cubic to a rhombohedral structure during sodiation, as confirmed by the peak analysis in the XRD pattern (Figure 2c). During sodiation, the synthesized NiHCF, which originally had representative features of a face-centered cubic structure similar to that of Prussian blue ($Fe_4[Fe(CN)_6]_3$ (JCPDS 52-1907)), was subject to rhombohedral distortion as indicated by the doublet peaks at the diffraction line indexes of 220, 420, 440, and 620.[40,43] NiHCF is a thoroughly studied material in aqueous Na-ion batteries and known to exhibit a high charge capacity (~60 mAh g^{-1}), rapid rate performance for sodium inter/deintercalation in an aqueous phase, and excellent stability in aqueous condition; thus, it was used as a suitable Na^+-capturing electrode for the MC-DB.[42,44−49]

Additionally, as shown in Figure 2d, the commercial Ag particles had a spherical rock shape with a randomly distributed particle size of 1−4 μm. The CV and XRD pattern of the Ag electrodes (Figure 2e,f) reveal that Ag underwent a rapid reversible chemical reaction with chloride ions to form AgCl. Rapid conversion from Ag to AgCl occurred at approximately 0.17 V (vs Ag/AgCl KCl sat.), whereas the reduction of AgCl to Ag occurred at −0.18 V (vs Ag/AgCl KCl sat.). The phase changes of the reversible conversion of Ag and AgCl were further supported by the XRD pattern of the chlorinated and dechlorinated Ag. In this study, NiHCF and Ag were used to formulate a MC-DB and operated according to the reversible electrochemical eqs 4 and 5 as follows

$$NaNi[Fe^{3+}(CN)_6] + xNa^+ + xe^- \rightarrow Na_{1+x}Ni[Fe^{3+}(CN)_6]_{1-x}[Fe^{2+}(CN)_6]_x \quad (4)$$

$$xAg + xCl^- \rightarrow xAgCl + xe^- \quad (5)$$

3.2. Desalination Performance: Constant Voltage Operation. The MC-DB provides a unique feature by independently controlling the surrounding condition of the electrodes from the target brackish water. Hence, solutions with different salinities can be supplied to each channel. Figure 3 shows the desalination performance of the MC-DB with a constant feed of 10 mM NaCl to investigate the effect of the side channel concentration ($F_{10}S_x$, x = 10−1000 mM). Note that the change in desalination capacity and average salt removal rate with respect to time is provided in Figure S2. As shown in Figure 3a, the growing amplitude of the conductivity profile change with an increase in side channel concentration indicated that more ions were removed and released during the desalination and regeneration steps as the feed concentration at the side channel increased. Accordingly, the desalination capacity increased from 17.4 to 52.9 mg g^{-1} with an increase in the maximum salt removal rate from 0.0191 to 0.0576 mg g^{-1} s^{-1} (production rate of 13.9−42.3 g m^{-2} h^{-1}) (Figure 3b). This threefold improvement in the desalination performance including desalination capacity and maximum salt removal rate implies that the MC-DB can provide a high performance even when treating brackish water with the key aspect of the MC-DB being the concentration gradient of the middle and side

DOI: 10.1021/acsami.9b10003
ACS Appl. Mater. Interfaces 2019, 11, 36580−36588

channels. The charge efficiency of the MC-DB system of all side channel concentrations were found to be close to unity (~98%), indicating that the MC-DB system was efficiently developed. In addition, the MC-DB ($F_{10}S_{1000}$) exhibited high cyclability by retaining 94.9% of the initial desalination capacity after 30 cycles (Figure S3, Supporting Information).

The performance improvement in the MC-DB system can be understood with the enhanced ion transport at the electrode−electrolyte interface. For example, considering a cation transport toward the NiHCF electrode, the cation needs to travel across the four main regions in the MC-DB system: low concentration solution, cation-exchange membrane, high-concentration solution, and the active materials in the electrodes (as illustrated in Figure S4, Supporting Information). There have been several reports indicating that the highly concentrated electrolyte can improve the rate of ion transport between the electrode and electrolyte interface.[29,50,51] Based on the cyclic voltammogram characterization of NiHCF (Figure S5, Supporting Information), the apparent diffusion coefficient was calculated using the Randles−Sevcik equation.[52] The diffusion coefficient of NiHCF rose from 5.9 × 10^{-11} to 1.5 × 10^{-10} m^2 s^{-1} as the surrounding electrolyte concentration increased from 10 to 1000 mM NaCl. In addition, as observed from the Nyquist plot shown in Figure S6, the highly concentrated solution in the side channel significantly reduced the total internal resistance. The series resistance (R_s) (e.g., ion-exchange membrane, electrolyte), which constitutes the major portion of the total internal resistance, decreased from 52.1 to 12.5 Ω. A prominent change was also observed in the charge-transfer resistance (R_{ct}). The R_{ct} decreased by 81.4% (15.8 to 2.93 Ω) as the side channel concentration increased from 10 to 1000 mM, indicating that the concentrated solution provided a much more favorable environment for the reversible reactions of Na^+ and Cl^- to occur at the battery electrodes.[53] The internal cell resistance of the MC-DB can be represented as the area-normalized equivalent series resistance (ANESR), which is an effective metric to compare the resistance of different cell configurations.[54] In this study, ANESR of the MC-DB operated with side channel concentrations of 10, 100, 500, and 1000 mM NaCl were measured to be 101, 109, 161, and 458 Ω cm^2, respectively.

Figure 4 shows the effect of cell voltage on the desalination performance of the MC-DB ($F_{10}S_{1000}$). The suitable range for constant-voltage operations of the MC-DB ($F_{10}S_{1000}$) was obtained through the CV characterization with the MC-DB cell (the two-electrode system) (Figure S7, Supporting Information). The CV shows broad reaction peaks over a voltage range from −1.5 to 1.5 V. The operational cell voltage of the system was set within a voltage range from −1.2 to 1.2 V to avoid side reactions such as oxygen and hydrogen evolution reactions. As shown in Figure 4a,b, the desalination capacity and average salt removal rate improved with the increase of the applied voltage. For example, as the applied voltage was changed from −0.8 to −1.2 V, the desalination capacity increased from 47 to 58 mg g^{-1} accompanied by an improvement in the maximum average salt removal rate from 0.0524 to 0.0595 mg g^{-1} s^{-1} (production rate of 36.6−46.3 g m^{-2} h^{-1}), respectively. This can be explained by an increased utilizable capacity of battery electrodes as a wider voltage range is applied. Although increasing the cell voltage results in improvement in the desalination performance, the energy consumed per salt removed increased significantly from 78.7 to

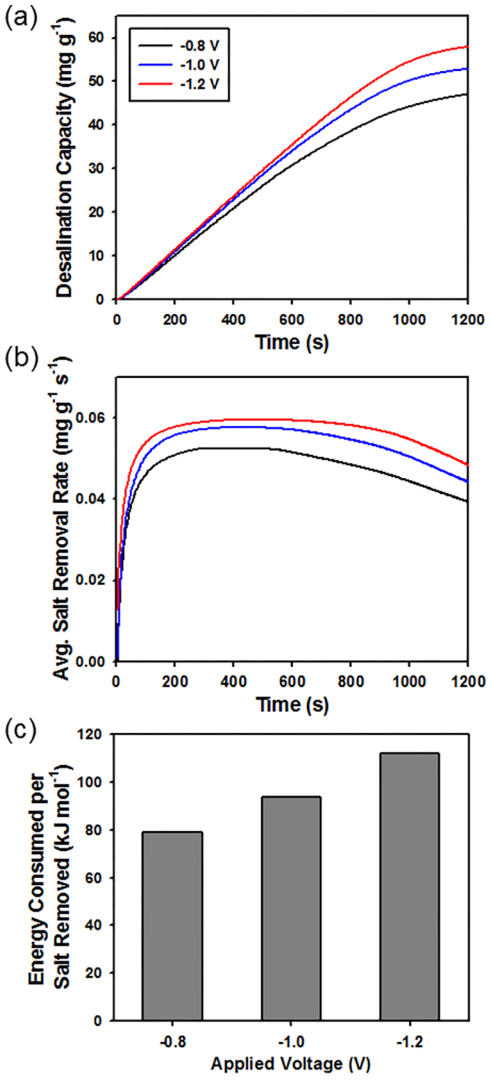


Figure 4. (a) Accumulated desalination capacity, (b) average salt removal rate, and (c) energy consumed per salt removed for the desalination step with various applied voltages ranging from −0.8 to −1.2 V under a $F_{10}S_{1000}$ condition.

111.8 kJ mol^{-1} as the operational voltage was changed from −0.8 V to −1.2 V (Figure 4c). Hence, there is a trade-off between the desalination capacity and the energy efficiency. To further optimize the MC-DB system, various operating parameters such as flow rate, duration of the desalination and regeneration steps, number of middle channels, and thickness of the channels should be investigated.

3.3. Desalination Performance: Constant-Current Operation. The MC-DB was further evaluated under a constant current operation to test the feasibility of the high current operation of the battery materials even when treating low-saline media such as brackish water. The CDI Ragone plot (Figure 5) effectively presents the capacity and rate performance of the electrochemical ion separation desalination systems.[55] Here, we show the desalination capacity and average salt removal rate, which was obtained by dividing the desalination capacity by the duration of the desalination step. As shown in Figure 5, a greater impact of the side channel concentration was observed on the desalination performance of the MC-DB at a high applied current (high salt removal rate) compared to a low applied current (low deionization

DOI: 10.1021/acsami.9b10003
ACS Appl. Mater. Interfaces 2019, 11, 36580−36588

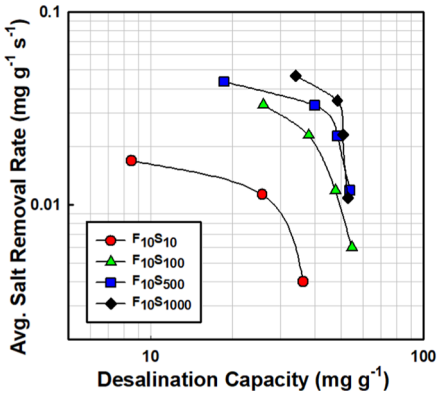


Figure 5. CDI Ragone plot obtained with a constant current operation (specific current of 5−40 A m^{-2}) with a cutoff voltage at −1.0 V. A desalination test was performed at a constant feed concentration of 10 mM NaCl in the middle channel with various feed concentrations for the side channel (S) ranging from 10 to 1000 mM ($F_{10}S_x$, x = 10−1000 mM) at a flow rate of 5 mL min^{-1}.

rate). For example, at a low applied current of 10 A m^{-2}, the MC-DB showed a high desalination capacity of approximately 25.7−52.8 mg g^{-1} under operating conditions from $F_{10}S_{10}$ to $F_{10}S_{1000}$. Meanwhile, at a high applied current operation, the capacity was significantly different from 8.5 mg g^{-1} at $F_{10}S_{10}$ to 34.1 mg g^{-1} at $F_{10}S_{1000}$. The high salinity in the side channel led to a greater capacity retention, which implies that the rate capability is significantly improved. This can be explained by the highly concentrated media in the side channel inducing a rapid ion diffusion by providing more available ions at the electrode−electrolyte interface. Note that at $F_{10}S_{10}$, the maximum operable current density was 15 A m^{-2}, whereas at $F_{10}S_{1000}$, the system could operate at a high current density of 40 A m^{-2}. This is a fast operation with a remarkable desalination capacity, even compared to the previous electrochemical desalination systems (constant current operation conditions of 2.8−20 A m^{-2}).[10−13,56−59] Despite the complexity of the MC-DB configuration, the performance of the battery electrodes are enhanced by improving the mass transfer at the electrode−electrolyte interface and reducing the system resistance. For the MC-DB to be used in practical application, further study regarding the scale up of the system should be conducted.

To further understand the superior desalination performance of the MC-DB based on concentration gradient, the effect of salinity on the electrochemical properties of the electrode materials was examined using a custom-designed electrochemical cell (Figure S8, Supporting Information). Figure 6a,b displays the potential curves of the NiHCF and Ag electrodes measured in the three-electrode system at various electrolyte concentrations (10−1000 mM NaCl) at a constant current of 10 A m^{-2}. As shown in the discharging curves (Figure 6a,b), the specific capacity increased from 30.5 to 58.0 mAh g^{-1} for the NiHCF electrode and 72.0 to 86.0 mAh g^{-1} for the Ag electrode. This enhancement was attributed to the presence of more accessible ions at the electrode−electrolyte interface as the electrolyte concentration increased. Note that as the

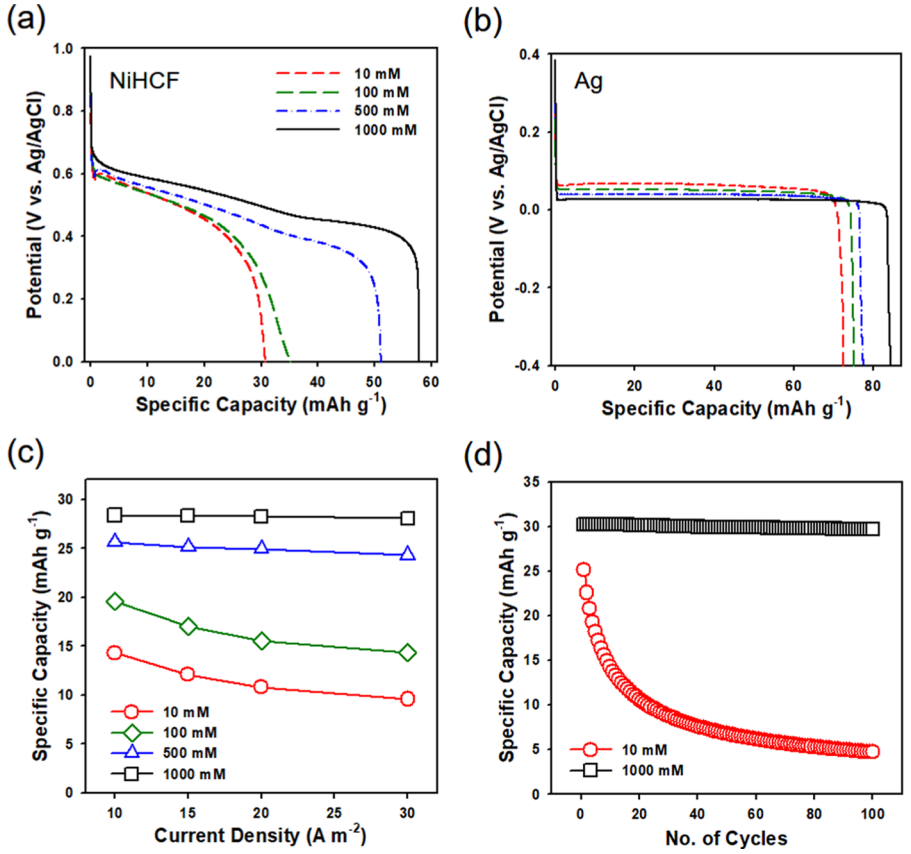


Figure 6. Galvanostatic discharging profiles for the (a) NiHCF and (b) Ag electrodes under different NaCl concentrations at a current density of 10 A m^{-2}. (c) Capacity retention of the NiHCF/Ag system at different current densities for various NaCl concentrations. (d) Capacity change of the NiHCF/Ag system cycled for 100 cycles in 10 and 1000 mM NaCl solutions at a current density of 30 A m^{-2}.

DOI: 10.1021/acsami.9b10003
ACS Appl. Mater. Interfaces 2019, 11, 36580−36588

electrolyte concentration increased, the specific capacity of the synthesized NiHCF reached close to the theoretical capacity of NiHCF and other PBA (~60 mAh g^{-1}).[44] On the other hand, the specific capacity of the Ag electrode only reached up to one-third of the theoretical capacity of Ag (248 mAh g^{-1}, assuming that one Ag atom reacts with one Cl atom). Perhaps, the Ag/AgCl conversion reaction may have remained only at the surface of the electrode. Although the specific capacity of the Ag electrode can be improved by increasing the surface area and enhancing the electronic conductivity of AgCl, more stable and low-cost anion-capturing electrodes are needed for practical application.

Figure 6c,d shows the galvanostatic performances and the cycling stability of the NiHCF/Ag system (two-electrode system) at various electrolyte concentrations. Figure 6c shows that the capacity retention of the NiHCF/Ag system improved with respect to the electrolyte concentration. As the charge and discharge rates increased from 10 to 30 A m^{-2}, the specific capacity decreased by 33.1, 26.7, 5.1, and 1.2% for the 10, 100, 500, and 1000 mM NaCl solutions, respectively, indicating that electrolyte concentration plays an important role in transporting ions as charge carriers. Furthermore, the electrolyte concentration also affects the cycle performance of the NiHCF/Ag system (Figure 6d). For example, after charging and discharging the system with a current density of 30 A m^{-2} for 100 cycles, an 81.3% capacity loss was observed for 10 mM NaCl, whereas only a 2.0% decrease was observed under the 1000 mM NaCl condition. This result was further investigated through the XRD characterization of the NiHCF electrodes (Figure S9, Supporting Information). The XRD spectra of the cycled NiHCF in the 1000 mM NaCl showed a negligible structural change compared to that of the pristine electrode, which are fully intercalated with Na^+. However, the doublet peaks in the 220, 420, 440, and 620 indexes changed to singlet peaks in the cycled NiHCF at 10 mM NaCl, indicating that the electrode is partially sodiated after cycling. This distinct change in the crystal structure could be related to an incomplete redox reaction because of the insufficient mass transfer of ions to the lattice structure when a potential difference is applied.

4. CONCLUSIONS

In this study, an MC-DB was successfully demonstrated as an effective design to mitigate the intrinsic mass-transfer limitation at the electrode−electrolyte interface, which is a key issue in treating brackish water using a DB. The MC-DB system consists of two side channels and a middle feed channel divided by cation- and anion-exchange membranes. The cell architecture allows one to provide a highly concentrated solution to the electrodes, which exhibit not only a high capacity but also enhanced rate capability. The MC-DB system showed a desalination capacity of 52.9 mg g^{-1} and a maximum salt removal rate of 0.0576 mg g^{-1} s^{-1} for the brackish water desalination (10 mM NaCl), approximately three times that under no concentration-gradient operation. In addition, the MC-DB deionized brackish water under a rapid operating condition (40.0 A m^{-2}) with a remarkable desalination capacity of 34.1 mg g^{-1}, notably fast even compared to the performances of the previously reported DB systems. From these results, we can infer that the MC-DB could be a viable system design to enhance the performance of DB by offering an optimal environment for the electrodes.

■ ASSOCIATED CONTENT

Supporting Information

The Supporting Information is available free of charge on the ACS Publications website at DOI: 10.1021/acsami.9b10003.

Schematics of the MC-DB and electrochemical characterization cell; supplementary characterizations; and experimental data of MC-DB including HRTEM, XRD, EIS, and cyclic voltammogram (PDF)

■ AUTHOR INFORMATION

Corresponding Author

*E-mail: jeyong@snu.ac.kr. Phone: +82-2-880-8927. Fax: +82-2-876-8911.

ORCID

Jaehan Lee: 0000-0002-8191-1396

Changha Lee: 0000-0002-0404-9405

Jeyong Yoon: 0000-0003-4455-3670

Author Contributions

⊥Jiho Lee and Jaehan Lee contributed equally to this work.

Notes

The authors declare no competing financial interest.

■ ACKNOWLEDGMENTS

This work was supported by the Technology Innovation Program (10082572, Development of Low Desalination Water Treatment Engineering Package System for Industrial Recycle Water Production) funded by the Ministry of Trade, Industry & Energy (MOTIE, Korea).

■ REFERENCES

(1) Xu, T.; Huang, C. Electrodialysis-based Separation Technologies: a Critical Review. *AIChE J.* **2008**, *54*, 3147−3159.

(2) Suss, M. E.; Porada, S.; Sun, X.; Biesheuvel, P. M.; Yoon, J.; Presser, V. Water Desalination via Capacitive Deionization: What Is It and What Can We Expect from It? *Energy Environ. Sci.* **2015**, *8*, 2296−2319.

(3) Yoon, H.; Lee, J.; Kim, S.; Yoon, J. Review of Concepts and Applications of Electrochemical Ion Separation (EIONS) Process. *Sep. Purif. Technol.* **2019**, *215*, 190−207.

(4) Porada, S.; Zhao, R.; Van Der Wal, A.; Presser, V.; Biesheuvel, P. Review on the Science and Technology of Water Desalination by Capacitive Deionization. *Prog. Mater. Sci.* **2013**, *58*, 1388−1442.

(5) Lee, J.; Kim, S.; Kim, C.; Yoon, J. Hybrid Capacitive Deionization to Enhance the Desalination Performance of Capacitive Techniques. *Energy Environ. Sci.* **2014**, *7*, 3683−3689.

(6) Biesheuvel, P. M.; van der Wal, A. Membrane Capacitive Deionization. *J. Membr. Sci.* **2010**, *346*, 256−262.

(7) Yoon, H.; Lee, J.; Kim, S.-R.; Kang, J.; Kim, S.; Kim, C.; Yoon, J. Capacitive Deionization with Ca-alginate Coated-carbon Electrode for Hardness Control. *Desalination* **2016**, *392*, 46−53.

(8) Lee, J.; Jo, K.; Lee, J.; Hong, S. P.; Kim, S.; Yoon, J. Rocking-Chair Capacitive Deionization for Continuous Brackish Water Desalination. *ACS Sustainable Chem. Eng.* **2018**, *6*, 10815−10822.

(9) Niu, J.; Conway, B. E.; Pell, W. G. Comparative Studies of Self-discharge by Potential Decay and Float-current Measurements at C Double-layer Capacitor and Battery Electrodes. *J. Power Sources* **2004**, *135*, 332−343.

(10) Kim, T.; Gorski, C. A.; Logan, B. E. Low Energy Desalination Using Battery Electrode Deionization. *Environ. Sci. Technol. Lett.* **2017**, *4*, 444−449.

(11) Lee, J.; Kim, S.; Yoon, J. Rocking Chair Desalination Battery based on Prussian Blue Electrodes. *ACS Omega* **2017**, *2*, 1653−1659.

(12) Porada, S.; Shrivastava, A.; Bukowska, P.; Biesheuvel, P.; Smith, K. C. Nickel Hexacyanoferrate Electrodes for Continuous Cation

Intercalation Desalination of Brackish Water. *Electrochim. Acta* **2017**, *255*, 369−378.
(13) Nam, D. H.; Choi, K.-S. Bismuth as a New Chloride-storage Electrode Enabling the Construction of a Practical High Capacity Desalination Battery. *J. Am. Chem. Soc.* **2017**, *139*, 11055−11063.
(14) Divyapriya, G.; Vijayakumar, K. K.; Nambi, I. Development of a Novel Graphene/Co_3O_4 Composite for Hybrid Capacitive Deionization System. *Desalination* **2019**, *451*, 102−110.
(15) Chen, F.; Huang, Y.; Guo, L.; Sun, L.; Wang, Y.; Yang, H. Y. Dual-ions Electrochemical Deionization: a Desalination Generator. *Energy Environ. Sci.* **2017**, *10*, 2081−2089.
(16) Pasta, M.; Wessells, C. D.; Cui, Y.; La Mantia, F. A Desalination Battery. *Nano Lett.* **2012**, *12*, 839−843.
(17) Huang, Y.; Chen, F.; Guo, L.; Zhang, J.; Chen, T.; Yang, H. Y. Low Energy Consumption Dual-ion Electrochemical Deionization System using $NaTi_2(PO_4)_3$-AgNPs Electrodes. *Desalination* **2019**, *451*, 241−247.
(18) Suss, M. E.; Presser, V. Water Desalination with Energy Storage Electrode Materials. *Joule* **2018**, *2*, 10−15.
(19) Tsouris, C.; Mayes, R.; Kiggans, J.; Sharma, K.; Yiacoumi, S.; DePaoli, D.; Dai, S. Mesoporous Carbon for Capacitive Deionization of Saline Water. *Environ. Sci. Technol.* **2011**, *45*, 10243−10249.
(20) Feng, C.; Chen, Y.-A.; Yu, C.-P.; Hou, C.-H. Highly Porous Activated Carbon with Multi-channeled Structure Derived from Loofa Sponge as a Capacitive Electrode Material for the Deionization of Brackish Water. *Chemosphere* **2018**, *208*, 285−293.
(21) Li, Y.; Kim, J.; Wang, J.; Liu, N.-L.; Bando, Y.; Alshehri, A. A.; Yamauchi, Y.; Hou, C.-H.; Wu, K. C. W. High Performance Capacitive Deionization using Modified ZIF-8-derived, N-doped Porous Carbon with Improved Conductivity. *Nanoscale* **2018**, *10*, 14852−14859.
(22) Jain, A.; Kim, J.; Owoseni, O. M.; Weathers, C.; Caña, D.; Zuo, K.; Walker, W. S.; Li, Q.; Verduzco, R. Aqueous-Processed, High-Capacity Electrodes for Membrane Capacitive Deionization. *Environ. Sci. Technol.* **2018**, *52*, 5859−5867.
(23) Yan, T.; Liu, J.; Lei, H.; Shi, L.; An, Z.; Park, H. S.; Zhang, D. Capacitive Deionization of Saline Water using Sandwich-like Nitrogen-doped Graphene Composites via a Self-assembling Strategy. *Environ. Sci.: Nano* **2018**, *5*, 2722−2730.
(24) Zhang, J.; Fang, J.; Han, J.; Yan, T.; Shi, L.; Zhang, D. N, P, S Co-doped Hollow Carbon Polyhedra Derived from MOF-based Core−shell Nanocomposites for Capacitive Deionization. *J. Mater. Chem. A* **2018**, *6*, 15245−15252.
(25) Khan, Z. U.; Yan, T.; Shi, L.; Zhang, D. Improved Capacitive Deionization by using 3D Intercalated Graphene Sheet−sphere Nanocomposite Architectures. *Environ. Sci.: Nano* **2018**, *5*, 980−991.
(26) Han, J.; Shi, L.; Yan, T.; Zhang, J.; Zhang, D. Removal of Ions from Saline Water using N, P Co-doped 3D Hierarchical Carbon Architectures via Capacitive Deionization. *Environ. Sci.: Nano* **2018**, *5*, 2337−2345.
(27) Hillel, D. *Salinity Management for Sustainable Irrigation: Integrating Science, Environment, and Economics*; The World Bank, 2000.
(28) Porada, S.; Shrivastava, A.; Bukowska, P.; Biesheuvel, P. M.; Smith, K. C. Nickel Hexacyanoferrate Electrodes for Continuous Cation Intercalation Desalination of Brackish Water. *Electrochim. Acta* **2017**, *255*, 369−378.
(29) Shanbhag, S.; Bootwala, Y.; Whitacre, J.; Mauter, M. Ion Transport and Competition Effects on $NaTi_2(PO_4)_3$ and $Na_4Mn_9O_{18}$ Selective Insertion Electrode Performance. *Langmuir* **2017**, *33*, 12580−12591.
(30) Yu, S. H.; Shokouhimehr, M.; Hyeon, T.; Sung, Y.-E. Iron Hexacyanoferrate Nanoparticles as Cathode Materials for Lithium and Sodium Rechargeable Batteries. *ECS Electrochem. Lett.* **2013**, *2*, A39−A41.
(31) Kim, D. K.; Muralidharan, P.; Lee, H.-W.; Ruffo, R.; Yang, Y.; Chan, C. K.; Peng, H.; Huggins, R. A.; Cui, Y. Spinel LiMn2O4 Nanorods as Lithium Ion Battery Cathodes. *Nano Lett.* **2008**, *8*, 3948−3952.
(32) Qu, Q.; Fu, L.; Zhan, X.; Samuelis, D.; Maier, J.; Li, L.; Tian, S.; Li, Z.; Wu, Y. Porous $LiMn_2O_4$ as Cathode Material with High Power and Excellent Cycling for Aqueous Rechargeable Lithium Batteries. *Energy Environ. Sci.* **2011**, *4*, 3985−3990.
(33) Luo, J.; Wang, Y.; Xiong, H.; Xia, Y. Ordered Mesoporous Spinel $LiMn_2O_4$ by a Soft-chemical Process as a Cathode Material for Lithium-ion Batteries. *Chem. Mater.* **2007**, *19*, 4791−4795.
(34) You, Y.; Yao, H. R.; Xin, S.; Yin, Y. X.; Zuo, T. T.; Yang, C. P.; Guo, Y. G.; Cui, Y.; Wan, L. J.; Goodenough, J. B. Subzero-Temperature Cathode for a Sodium-Ion Battery. *Adv. Mater.* **2016**, *28*, 7243−7248.
(35) Huang, Y.; Chen, F.; Guo, L.; Yang, H. Y. Ultrahigh Performance of a Novel Electrochemical Deionization System based on a $NaTi_2(PO_4)_3$/rGO Nanocomposite. *J. Mater. Chem. A* **2017**, *5*, 18157−18165.
(36) Wang, H.; Wang, L.; Chen, S.; Li, G.; Quan, J.; Xu, E.; Song, L.; Jiang, Y. Crystallographic-plane Tuned Prussian-blue Wrapped with RGO: a High-capacity, Long-life Cathode for Sodium-ion Batteries. *J. Mater. Chem. A* **2017**, *5*, 3569−3577.
(37) Kim, C.; Lee, J.; Srimuk, P.; Aslan, M.; Presser, V. Concentration-Gradient Multichannel Flow-Stream Membrane Capacitive Deionization Cell for High Desalination Capacity of Carbon Electrodes. *ChemSusChem* **2017**, *10*, 4914−4920.
(38) Kim, C.; Srimuk, P.; Lee, J.; Aslan, M.; Presser, V. Semi-continuous Capacitive Deionization using Multi-channel Flow Stream and Ion Exchange Membranes. *Desalination* **2018**, *425*, 104−110.
(39) Kim, C.; Srimuk, P.; Lee, J.; Presser, V. Enhanced Desalination via Cell Voltage Extension of Membrane Capacitive Deionization using an Aqueous/Organic Bi-electrolyte. *Desalination* **2018**, *443*, 56−61.
(40) Wu, X.; Sun, M.; Guo, S.; Qian, J.; Liu, Y.; Cao, Y.; Ai, X.; Yang, H. Vacancy-Free Prussian Blue Nanocrystals with High Capacity and Superior Cyclability for Aqueous Sodium-Ion Batteries. *ChemNanoMat* **2015**, *1*, 188−193.
(41) Choi, S.; Chang, B.; Kim, S.; Lee, J.; Yoon, J.; Choi, J. W. Battery Electrode Materials with Omnivalent Cation Storage for Fast and Charge-Efficient Ion Removal of Asymmetric Capacitive Deionization. *Adv. Funct. Mater.* **2018**, *28*, No. 1802665.
(42) Yang, D.; Xu, J.; Liao, X. Z.; He, Y. S.; Liu, H.; Ma, Z.-F. Structure Optimization of Prussian Blue Analogue Cathode Materials for Advanced Sodium Ion Batteries. *Chem. Commun.* **2014**, *50*, 13377−13380.
(43) Ren, W.; Qin, M.; Zhu, Z.; Yan, M.; Li, Q.; Zhang, L.; Liu, D.; Mai, L. Activation of Sodium Storage Sites in Prussian Blue Analogues via Surface Etching. *Nano Lett.* **2017**, *17*, 4713−4718.
(44) Wessells, C. D.; Peddada, S. V.; Huggins, R. A.; Cui, Y. Nickel Hexacyanoferrate Nanoparticle Electrodes for Aqueous Sodium and Potassium Ion Batteries. *Nano Lett.* **2011**, *11*, 5421−5425.
(45) Wang, R. Y.; Shyam, B.; Stone, K. H.; Weker, J. N.; Pasta, M.; Lee, H. W.; Toney, M. F.; Cui, Y. Reversible Multivalent (Monovalent, Divalent, Trivalent) Ion Insertion in Open Framework Materials. *Adv. Energy Mater.* **2015**, *5*, No. 1401869.
(46) Lu, Y.; Wang, L.; Cheng, J.; Goodenough, J. B. Prussian Blue: a New Framework of Electrode Materials for Sodium Batteries. *Chem. Commun.* **2012**, *48*, 6544−6546.
(47) Chen, L.; Zhang, L.; Zhou, X.; Liu, Z. Aqueous Batteries based on Mixed Monovalence Metal Ions: a New Battery Family. *ChemSusChem* **2014**, *7*, 2295−2302.
(48) You, Y.; Wu, X.-L.; Yin, Y.-X.; Guo, Y.-G. High-quality Prussian Blue Crystals as Superior Cathode Materials for Room-temperature Sodium-ion Batteries. *Energy Environ. Sci.* **2014**, *7*, 1643−1647.
(49) Cai, D.; Yang, X.; Qu, B.; Wang, T. Comparison of the Electrochemical Performance of Iron Hexacyanoferrate with High and Low Quality as Cathode Materials for Aqueous Sodium-ion Batteries. *Chem. Commun.* **2017**, *53*, 6780−6783.
(50) Kim, D. J.; Ponraj, R.; Kannan, A. G.; Lee, H.-W.; Fathi, R.; Ruffo, R.; Mari, C. M.; Kim, D. K. Diffusion Behavior of Sodium Ions in $Na_{0.44}MnO_2$ in Aqueous and Non-aqueous Electrolytes. *J. Power Sources* **2013**, *244*, 758−763.

DOI: 10.1021/acsami.9b10003
ACS Appl. Mater. Interfaces 2019, 11, 36580−36588

(51) He, P.; Zhang, X.; Wang, Y.-G.; Cheng, L.; Xia, Y.-Y. Lithium-ion Intercalation Behavior of $LiFePO_4$ in Aqueous and Nonaqueous Electrolyte Solutions. *J. Electrochem. Soc.* **2008**, *155*, A144−A150.
(52) Bard, A. J.; Faulkner, L. R.; Leddy, J.; Zoski, C. G. *Electrochemical Methods: Fundamentals and Applications*; Wiley: New York, 1980.
(53) Tatara, R.; Karayaylali, P.; Yu, Y.; Zhang, Y.; Giordano, L.; Maglia, F.; Jung, R.; Schmidt, J. P.; Lund, I.; Shao-Horn, Y. The Effect of Electrode-Electrolyte Interface on the Electrochemical Impedance Spectra for Positive Electrode in Li-Ion Battery. *J. Electrochem. Soc.* **2019**, *166*, A5090−A5098.
(54) Qu, Y.; Baumann, T. F.; Santiago, J. G.; Stadermann, M. Characterization of Resistances of a Capacitive Deionization System. *Environ. Sci. Technol.* **2015**, *49*, 9699−9706.
(55) Kim, T.; Yoon, J. CDI Ragone Plot as a Functional Tool to Evaluate Desalination Performance in Capacitive Deionization. *RSC Adv.* **2015**, *5*, 1456−1461.
(56) Długołęcki, P.; van der Wal, A. Energy Recovery in Membrane Capacitive Deionization. *Environ. Sci. Technol.* **2013**, *47*, 4904−4910.
(57) García-Quismondo, E.; Gómez, R.; Vaquero, F.; Cudero, A. L.; Palma, J.; Anderson, M. New Testing Procedures of a Capacitive Deionization Reactor. *Phys. Chem. Chem. Phys.* **2013**, *15*, 7648−7656.
(58) Jande, Y.; Kim, W.-S. Desalination using Capacitive Deionization at Constant Current. *Desalination* **2013**, *329*, 29−34.
(59) García-Quismondo, E.; Santos, C.; Lado, J.; Palma, J.; Anderson, M. A. Optimizing the Energy Efficiency of Capacitive Deionization Reactors Working under Real-world Conditions. *Environ. Sci. Technol.* **2013**, *47*, 11866−11872.

DOI: 10.1021/acsami.9b10003
ACS Appl. Mater. Interfaces 2019, 11, 36580−36588